Dynamic Response of an Aerial Rescue Ladder under Wind Gust Loading

Xiaoyang Zhao, Shixuan Sun

December 11, 2025

Abstract

Aerial rescue ladders are long, slender and lightly damped structures whose dynamic response can be strongly affected by wind gusts when fully extended. Large tip motions under cross-wind compromise operator safety and positioning accuracy, while systematic full-scale testing during real operations is impractical. This project therefore develops a mechanically consistent numerical model to study wind–induced vibration of a 20 m aerial ladder equipped with a passive torsional spring–damper at the turntable base. The ladder is idealised as a planar discretised Euler–Bernoulli beam (Cosserat-rod formulation) with lumped masses, Rayleigh damping and a finite-duration lateral wind load obtained from a bluff-body drag law. Three wind speeds, $U = 5, 10, 15$ m/s (Reynolds numbers $\mathrm{Re} \approx 10^5$–3.1×10^5), are simulated using fully implicit time integration. The predicted peak horizontal tip deviations are approximately 0.2, 0.6 and 1.3 m, respectively, followed by decay to within a few centimetres of the new equilibrium position within 10–12 s. Base rotation remains small ($< 0.3^\circ$) in all cases, indicating that deformation is dominated by bending along the span. Overall, the results suggest that the chosen passive base damping substantially attenuates gust-induced oscillations for moderate winds, but that strong cross-winds can still generate large tip excursions. The passive configuration thus provides a practical baseline for evaluating potential semi-active or active damping strategies in future work.

1 Introduction

1.1 Problem Statement

In modern firefighting and rescue operations, aerial ladders are routinely deployed to transport personnel and equipment from ground level to elevated working positions such as building façades and roofs. When the ladder is fully extended, it becomes a long, slender and lightly damped structure, and its dynamic response is strongly influenced by environmental disturbances. In particular, wind gusts acting over the exposed span can excite significant lateral vibration and oscillatory motion of the rescue cage, which compromises both operator comfort and safety. Additional disturbances may arise from base motion of the fire truck, sudden load changes due to personnel movement, or emergency manoeuvres.

These effects are difficult to study experimentally during real operations because of safety, cost and repeatability constraints. It is therefore useful to construct a numerical model that can reproduce the essential dynamics of an extended aerial ladder under realistic loading, and to use this model to evaluate practical vibration–mitigation strategies. In this project, the focus is placed on a simple but physically meaningful configuration: a multi-segment flexible ladder with a passive torsional spring–damper at the base and a distributed wind load acting along the ladder span. The goal is to quantify how wind speed and base damping influence tip displacement and base rotation, and to assess whether such a passive system provides sufficient vibration suppression for typical operating conditions.

Figure 1: Aerial ladder mounted on a fire truck during high-altitude operation.

1.2 Aims and Objectives

The overall aim of this project is to study the wind–induced vibration of an extended aerial ladder and to assess how far a passive base damping system can reduce the resulting structural oscillations. The analysis is carried out using a simplified but mechanically consistent dynamic model that is excited by aerodynamic loads derived from basic bluff–body theory.

To address this aim, the project pursues the following objectives:

- **Formulate a simplified dynamic model of the aerial ladder.** Idealise the ladder as a planar, flexible Euler–Bernoulli beam (Cosserat-rod style discretisation) with lumped masses and gravity loading. Represent the connection to the fire-truck turntable by a torsional spring–damper at the base joint.
- **Represent wind loading through a distributed aerodynamic force.** Model the incoming wind as a uniform lateral flow of prescribed speed and compute an equivalent distributed load along the ladder using a bluff–body drag expression, parameterised by Reynolds number and drag coefficient.
- **Compute the vibration response under a finite-duration gust.** Use an implicit time-integration scheme to obtain time histories of tip displacement, base rotation and internal forces when the ladder is exposed to a transient wind input and then allowed to vibrate freely.
- **Perform a parametric study in wind speed.** Simulate several wind-speed cases and compare the resulting peak tip deflections, decay rates and residual deformations in order to quantify the sensitivity of the ladder response to cross-wind intensity.
- **Interpret the results from a design and operation perspective.** Relate the numerical findings to practical issues such as acceptable tip motion, safe operating wind speeds and the apparent effectiveness of the chosen passive base damping, and outline how the model could be extended to future semi-active or active damping strategies.

2 Literature Review

2.1 Background and Research Motivation

Modern aerial ladder systems used in firefighting are known to be highly susceptible to environmental disturbances when operated at large outreach and elevation angles. Horváth et al. (2020) reported that sudden wind gusts can cause lateral deflections on the order of one metre at the ladder tip under maximum extension and loading, creating a serious operational risk for firefighters in the rescue cage [1]. Such large-amplitude oscillations not only reduce positional accuracy but can also lead to loss of balance or collision with nearby structures.

These observations motivate the need for reliable vibration-mitigation strategies, ranging from purely passive measures (structural stiffness, damping and mass distribution) to more advanced active or semi-active control systems. For practical deployment on fire trucks, any proposed solution must be robust, mechanically simple and compatible with limited sensor and controller resources, while still offering meaningful reductions in vibration amplitude under realistic wind conditions.

2.2 Modelling Approaches in Ladder Dynamics and Vibration Control

Several modelling and control strategies have been proposed in the literature for flexible structures that are similar in spirit to aerial ladders. Lavassani et al. (2025) investigated semi-active vibration control of offshore jacket platforms using a semi-active tuned mass damper inerter (SATMDI) controlled by a feedback algorithm [2]. Their work shows that measuring the structural response in real time and adjusting the damping device accordingly can significantly reduce the response to stochastic wind and wave loading. Although the application is marine, the concept of feedback-regulated energy dissipation is directly relevant to the problem of stabilising slender ladder structures under wind excitation.

Closer to the present application, Kharitonov et al. (2007) modelled a fire-rescue turntable ladder as an Euler–Bernoulli beam with a concentrated end mass representing the rescue cage, and derived analytical eigenfunctions to obtain a low-order modal representation of the system [3]. Using strain-gauge and gyroscope measurements, the authors designed a feedback controller capable of damping the fundamental and first overtone modes, achieving stable operation for ladder lengths exceeding 30 m. Their results demonstrate that even relatively simple feedback laws, when combined with an appropriate structural model, can effectively suppress dominant vibration modes.

Other researchers have proposed control strategies based on multibody dynamics or flexible-manipulator theory. Aschemann et al. (2002) developed a trajectory control method for fire-rescue ladders using a multibody model and decentralised feedback, which successfully reduced the main oscillation mode but remained less effective for higher modes at large extensions [4]. Zuyev and Sawodny (2005) studied the stabilisation of flexible manipulators with passive joints using Galerkin approximations and Lyapunov-based feedback design [5]. While these approaches offer strong theoretical guarantees, they typically require significant computational effort and sophisticated sensing, which can be challenging to implement on resource-constrained embedded hardware.

Beyond ladder-specific studies, general control theory emphasises the advantages of closed-loop feedback for systems exposed to uncertain dynamics and disturbances. As Frank (2018) notes, closed-loop control enables a system to compensate for incomplete knowledge of the plant and to reject unpredictable perturbations by continually adjusting the control input based on measured output [6]. This principle underpins many modern active and semi-active vibration-control schemes.

2.3 Identified Gaps and Present Focus

The literature indicates that active and semi-active control methods can substantially improve the dynamic performance of flexible structures such as aerial ladders. However, most existing implementations either rely on detailed modal models and complex state estimation, or require specialised hardware such as magnetorheological dampers and high-performance controllers. For fire-service applications, where robustness, ease of maintenance and cost are critical, there is still a need for simpler control concepts that can be integrated into existing ladder designs with minimal additional equipment.

In this context, the present work deliberately adopts a reduced-order yet physically informed modelling strategy. The aerial ladder is approximated as a discretised Euler–Bernoulli beam with distributed mass and a passive torsional spring–damper at the base. Wind loading is modelled as a spatially uniform distributed drag load derived from classical bluff-body aerodynamics, parameterised by wind speed and Reynolds number. This setting allows a systematic numerical study of how environmental conditions and base damping influence tip displacement and base rotation, while keeping the model computationally inexpensive and suitable for real-time simulation.

Rather than implementing a full semi-active or active controller, this project focuses on carefully characterising the passive response and identifying regimes in which passive base damping already provides adequate vibration suppression. The insights gained from this baseline study form a natural foundation for future work, in which a feedback-based semi-active law—conceptually inspired by the strategies of Lavassani et al. (2025) and Kharitonov et al. (2007)—could be added to modulate the base damping in real time. In this way, the present report bridges the gap between purely passive design and more sophisticated control-oriented approaches, while remaining closely aligned with practical constraints of aerial ladder operation.

3 Methodology

3.1 Implementation Overview

The dynamic response of the aerial ladder is simulated using a discrete Cosserat–rod (Euler–Bernoulli beam) formulation with lumped masses at the nodes. The ladder is modelled as a planar, flexible beam of finite length, hinged at the turntable and equipped with a passive torsional spring–damper at its base.

Environmental loading is represented by a lateral wind gust acting along the projected span of the ladder. The gust is modelled as a finite–duration distributed load derived from a bluff–body drag expression, parameterised by wind speed and Reynolds number. For each wind speed case, the nonlinear equations of motion are integrated in time using a fully implicit scheme, and the resulting tip displacement, base rotation and deformed shapes are used to assess the effectiveness of the passive base damping.

Although the literature review motivates semi–active and active damping strategies, the present implementation focuses on a purely passive configuration. The passive baseline is first characterised in detail, and the results then serve as a reference for discussing possible semi–active extensions in future work.

3.2 Geometric Modelling of the Ladder

The aerial ladder is idealised as a slender flexible beam of total length

$$L = 20 \text{ m},$$

initially inclined at

$$\theta_0 = 60^\circ$$

with respect to the horizontal. The centreline is discretised into

$$N = 51$$

nodes, yielding $N - 1 = 50$ uniform segments of length

$$\Delta L = \frac{L}{N-1} = 0.4 \text{ m}.$$

Each node carries two in–plane translational degrees of freedom,

$$q = [x_0, y_0, x_1, y_1, \ldots, x_{N-1}, y_{N-1}]^T \in \mathbb{R}^{2N},$$

so that the total number of degrees of freedom is $2N = 102$. The first two nodes are clamped to represent the rigid connection between the ladder base and the turntable; their four translational DOFs are held fixed in time, while the remaining DOFs are treated as free.

3.3 Effective Cross–Section and Material Properties

Rather than resolving the detailed truss geometry of a real fire–rescue ladder, an equivalent homogeneous beam is used. The ladder is assumed to be made of lightweight aluminium alloy with Young's modulus

$$E_{\text{alloy}} = 70 \text{ GPa}.$$

An effective bending stiffness

$$EI_{\text{eff}} \approx 8.0 \times 10^5 \text{ N m}^2$$

is chosen to be representative of a typical extended aerial ladder segment. This value is used directly in the bending energy term of the Cosserat–beam formulation.

To supply a finite axial stiffness, an effective axial area A_{eff} is prescribed and the axial rigidity is set to

$$EA = E_{\text{alloy}}\, A_{\text{eff}},$$

with $A_{\text{eff}} = 0.04\ \text{m}^2$ in the simulations. This choice ensures that the ladder primarily responds in bending, while still allowing the stretching energy to stabilise the numerical scheme.

A lumped mass model is adopted for inertia. Each node is assigned a notional spherical mass of radius

$$R_k = \frac{\Delta L}{10} = 0.04\ \text{m},$$

with density

$$\rho = 2700\ \text{kg/m}^3,$$

leading to a nodal mass

$$m_k = \frac{4}{3}\pi R_k^3 \rho, \qquad k = 0, \ldots, N-1.$$

To emulate the presence of additional equipment or a firefighter load, the radius R_k (and therefore the mass) of the mid–span node is increased in the numerical model. In this way the total mass distribution more closely reflects an operational ladder with a basket and payload.

3.4 Discrete Elastic Energy Formulation

The internal elastic forces are obtained from a discrete energy formulation consistent with a planar Cosserat–rod or Euler–Bernoulli beam. For each segment between nodes k and $k+1$, the stretching energy is defined as

$$E_s^{(k)} = \frac{EA}{2}\left(\frac{\ell_k - \Delta L}{\Delta L}\right)^2, \qquad \ell_k = \|\mathbf{x}_{k+1} - \mathbf{x}_k\|,$$

where $\mathbf{x}_k = (x_k, y_k)$ is the position vector of node k. This penalises deviation of the segment length ℓ_k from the reference length ΔL.

Bending is measured via a discrete curvature defined on each triplet of nodes $(k-1, k, k+1)$. The unit tangents

$$\mathbf{t}_{k-1} = \frac{\mathbf{x}_k - \mathbf{x}_{k-1}}{\|\mathbf{x}_k - \mathbf{x}_{k-1}\|}, \qquad \mathbf{t}_k = \frac{\mathbf{x}_{k+1} - \mathbf{x}_k}{\|\mathbf{x}_{k+1} - \mathbf{x}_k\|},$$

are used to construct the scalar curvature

$$\kappa_k = \left[2\frac{\mathbf{t}_{k-1} \times \mathbf{t}_k}{1 + \mathbf{t}_{k-1} \cdot \mathbf{t}_k}\right]_z,$$

where $[\cdot]_z$ denotes the out–of–plane component. The bending energy associated with node k is then

$$E_b^{(k)} = \frac{EI_{\text{eff}}}{2}(\kappa_k - \kappa_0)^2, \qquad \kappa_0 = 0,$$

corresponding to a straight reference configuration.

The total elastic energy

$$E_{\text{elastic}} = \sum_k E_s^{(k)} + \sum_k E_b^{(k)}$$

gives rise to internal forces and tangent stiffness matrices via

$$\mathbf{F}_{\text{elastic}}(q) = -\nabla_q E_{\text{elastic}}, \qquad \mathbf{K}_{\text{elastic}}(q) = \nabla_q^2 E_{\text{elastic}},$$

which are assembled from the segment and curvature contributions in the usual finite–element manner. This formulation is consistent with the `objfun` routine used in the numerical implementation.

3.5 Dynamic Model and Time Integration

The semi–discrete equations of motion of the ladder are written as

$$M\ddot{q} + C\dot{q} + \mathbf{F}_{\text{elastic}}(q) = W_{\text{ext}}(t),$$

where:

- $M = \text{diag}(m_0, m_0, m_1, m_1, \ldots, m_{N-1}, m_{N-1})$ is the diagonal lumped mass matrix;
- $C = \alpha_M M$ is a Rayleigh mass–proportional damping matrix, with $\alpha_M = 0.001$ chosen to introduce a modest amount of structural damping;
- $\mathbf{F}_{\text{elastic}}(q)$ is the nonlinear internal force vector obtained from the stretching and bending energies;
- $W_{\text{ext}}(t)$ collects all external loads, including gravity, the base torsional spring–damper forces, and wind–induced distributed loads.

A fully implicit Euler time integration scheme is used. Denoting velocity by $u = \dot{q}$, the update from step n to $n+1$ is

$$q_{n+1} = q_n + \Delta t\, u_{n+1}, \qquad u_{n+1} = u_n + \Delta t\, \ddot{q}_{n+1},$$

with $\ddot{q}_{n+1}$ obtained from the discretised equations of motion. At each time step, the nonlinear residual

$$\mathbf{f}(q_{n+1}) = M\frac{u_{n+1} - u_n}{\Delta t} + Cu_{n+1} + \mathbf{F}_{\text{elastic}}(q_{n+1}) - W_{\text{ext}}(t_{n+1})$$

is driven to zero using Newton–Raphson iterations and the corresponding Jacobian (tangent stiffness) assembled from the mass, damping and elastic terms. The time step is chosen as $\Delta t = 0.02$ s, and convergence is enforced with a residual tolerance of 10^{-3}.

3.6 Passive Base Joint Model

The ladder is connected to the fire–truck turntable through a rotationally flexible joint, modelled as a torsional spring–damper acting between nodes 1 and 2. Let ϕ denote the instantaneous angle of the first beam segment (from node 1 to node 2) with respect to the horizontal, and ϕ_0 the corresponding angle in the initial configuration. The relative rotation is

$$\phi - \phi_0,$$

and its time derivative $\dot{\phi}$ is computed from the nodal velocities.

The torsional moment at the base is represented as

$$M_\theta = -k_\theta(\phi - \phi_0) - c_\theta\dot{\phi},$$

with constant stiffness and damping values

$$k_\theta = 3.0 \times 10^4 \text{ N m/rad}, \qquad c_\theta = 1500 \text{ N m s/rad}.$$

This moment is converted into an equivalent pair of equal and opposite lateral forces at nodes 1 and 2 using the current segment length and normal direction. The resulting nodal forces enter $W_{\text{ext}}(t)$ at every time step. Since k_θ and c_θ are fixed, the base joint in this study is purely passive, without any active modulation.

3.7 Wind Loading Model and Reynolds Number

Wind is treated as a steady, uniform flow impinging laterally on the ladder. For a given wind speed U, the flow induces a drag force on the projected frontal area of the ladder, here modelled through a bluff–body drag expression. An effective lateral width

$$D = 0.30 \text{ m}$$

is used to represent the overall width of the ladder in the wind direction. For air density $\rho_{\text{air}} = 1.225 \text{ kg/m}^3$ and dynamic viscosity $\mu_{\text{air}} = 1.8 \times 10^{-5}$ Pa s, the Reynolds number is

$$\text{Re} = \frac{\rho_{\text{air}} U D}{\mu_{\text{air}}}.$$

A piecewise drag coefficient C_d is adopted to reflect the dependence on Re:

$$C_d = \begin{cases} 1.2, & \text{Re} < 2 \times 10^5, \\ 1.0, & 2 \times 10^5 \le \text{Re} < 4 \times 10^5, \\ 0.9, & \text{Re} \ge 4 \times 10^5. \end{cases}$$

The total lateral drag force on the ladder is then approximated by

$$F_{D,\text{total}} = \frac{1}{2} \rho_{\text{air}} U^2 C_d D L.$$

This is converted into a uniform distributed load along the span,

$$w_{\text{dist}} = \frac{F_{D,\text{total}}}{L} \quad [\text{N/m}],$$

which is subsequently discretised as nodal forces. In the numerical implementation, nodes from the second segment to the tip share the load via

$$F_{x,k} = w_{\text{dist}} \Delta L,$$

applied in the global horizontal direction at each node k.

To mimic a wind gust rather than a permanently sustained crosswind, the distributed load is applied only during a finite excitation window $0 \le t \le 4$ s, after which it is removed and the ladder is allowed to vibrate freely under gravity and base damping. Three wind speeds are investigated,

$$U = 5,\ 10,\ 15 \text{ m/s},$$

which correspond to Reynolds numbers of approximately

$$\text{Re}_5 \approx 1.0 \times 10^5, \qquad \text{Re}_{10} \approx 2.0 \times 10^5, \qquad \text{Re}_{15} \approx 3.1 \times 10^5.$$

These lie in the subcritical to transitional regime for flow past a bluff body, where the drag coefficient is only weakly sensitive to the exact Reynolds number, so the piecewise–constant C_d model is sufficient for the present study.

For each wind speed case, the time histories of tip displacement, base angle and representative nodal forces are recorded, together with snapshots of the deformed ladder shape at selected times

$$t = 0,\ 2,\ 4,\ 8,\ 12,\ 20 \text{ s},$$

in order to visualise the build–up and subsequent decay of oscillations under wind loading.

4 Results and Discussion

4.1 Wind loading and Reynolds number

For each prescribed wind speed $U = 5,\ 10,\ 15$ m/s the corresponding Reynolds number, drag coefficient and equivalent distributed load were computed using the bluff–body drag model described in Section 3.7. The resulting values are

$$\mathrm{Re}(5\ \mathrm{m/s}) \approx 1.0 \times 10^5, \qquad \mathrm{Re}(10\ \mathrm{m/s}) \approx 2.0 \times 10^5, \qquad \mathrm{Re}(15\ \mathrm{m/s}) \approx 3.1 \times 10^5.$$

In all three cases the flow is in the transitional/turbulent regime around a bluff body. The piecewise drag law yields

$$C_d \approx 1.20 \quad (\mathrm{Re} \approx 1.0 \times 10^5), \qquad C_d \approx 1.00 \quad (\mathrm{Re} \gtrsim 2.0 \times 10^5),$$

and the total steady drag forces on the extended ladder are

$$F_{D,\mathrm{total}} \approx 110.2,\ 367.5,\ 826.9\ \mathrm{N} \quad \text{for } U = 5,\ 10,\ 15\ \mathrm{m/s},$$

respectively. When converted into a uniform line load, these correspond to

$$w_{\mathrm{dist}} \approx 5.5,\ 18.4,\ 41.3\ \mathrm{N/m},$$

and to nodal forces of approximately 2.2, 7.4 and 16.5 N per node along the span. These values are of realistic magnitude for a 20 m aerial ladder subject to moderate to strong cross-wind, and they provide the basis for the subsequent dynamic simulations.

4.2 Tip displacement response

Figure 2 shows the horizontal tip displacement as a function of time for the three wind speeds. For all cases the wind load is applied between $t = 0$ and $t = 4$ s and then removed, after which the ladder undergoes free vibration under gravity and base damping.

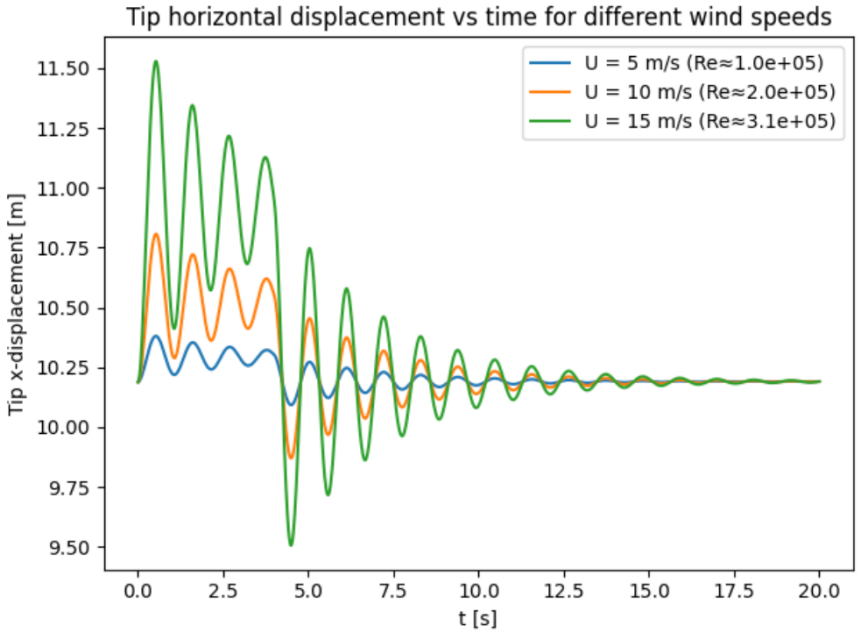

Figure 2: Horizontal tip displacement for three wind speeds.

During the excitation phase the tip displacement grows rapidly and exhibits small-amplitude oscillations superposed on a mean drift in the wind direction. The peak excursion increases systematically with wind speed: the post-processed maximum deviations from the long–time equilibrium position are approximately

$$\max |x_{\text{tip}} - x_{\text{eq}}| \approx 0.2,\ 0.6,\ 1.3 \text{ m} \quad \text{for } U = 5,\ 10,\ 15 \text{ m/s},$$

as summarised in Figure 3. The scaling is slightly stronger than linear in U, consistent with the fact that the aerodynamic force scales as U^2 while geometric and inertial nonlinearities modify the purely quadratic trend over this relatively narrow wind-speed range.

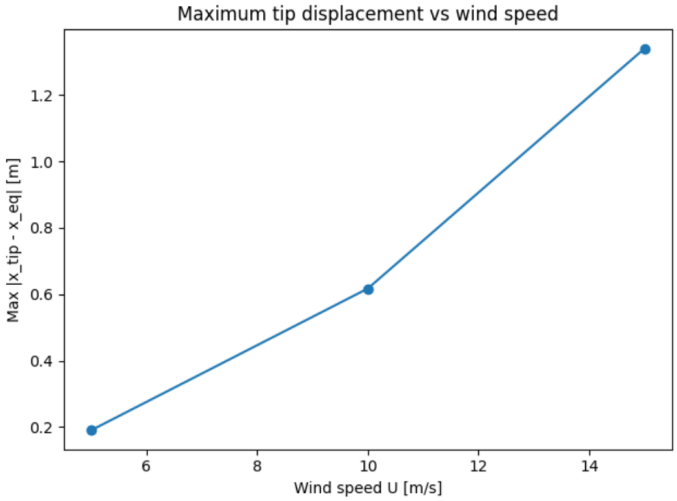

Figure 3: Maximum horizontal tip displacement versus wind speed.

After $t \approx 5$–6 s the external wind load has vanished and the response is dominated by damped free vibrations around a new static equilibrium position. The oscillation amplitude decays to less than 0.05 m within roughly 10–12 s for all three wind speeds, indicating that the combination of Rayleigh structural damping and the passive base torsional damper is sufficient to dissipate most of the gust-induced energy over a time scale that is short compared with typical rescue operations. This behaviour is qualitatively consistent with experimental observations in the literature, where tip swings of the order of one metre have been reported under strong gusts for extended ladders.

4.3 Base rotation response

The evolution of the base-segment angle $\phi(t)$, plotted in Figure 4, mirrors the features of the tip displacement but with much smaller absolute variation. The mean base angle remains close to the initial value $\phi_0 \approx 1.046$ rad and the dynamic fluctuation is only of the order of

$$|\phi(t) - \phi_0| \lesssim 0.005 \text{ rad} \quad (\approx 0.3^\circ)$$

even for the largest wind case. This confirms that the prescribed torsional stiffness $k_\theta = 3.0 \times 10^4$ N m/rad is high enough that the turntable joint behaves almost rigidly, with the majority of the lateral deflection taken up by bending along the ladder span rather than by rotation at the base.

The decay of base-angle oscillations is again clearly visible: higher wind speeds produce larger initial overshoots when the load is suddenly removed at $t = 4$ s, but all three cases converge to nearly identical steady angles by $t \approx 15$–20 s. This suggests that increasing the damping coefficient c_θ primarily affects the transient decay rate rather than the final equilibrium orientation.

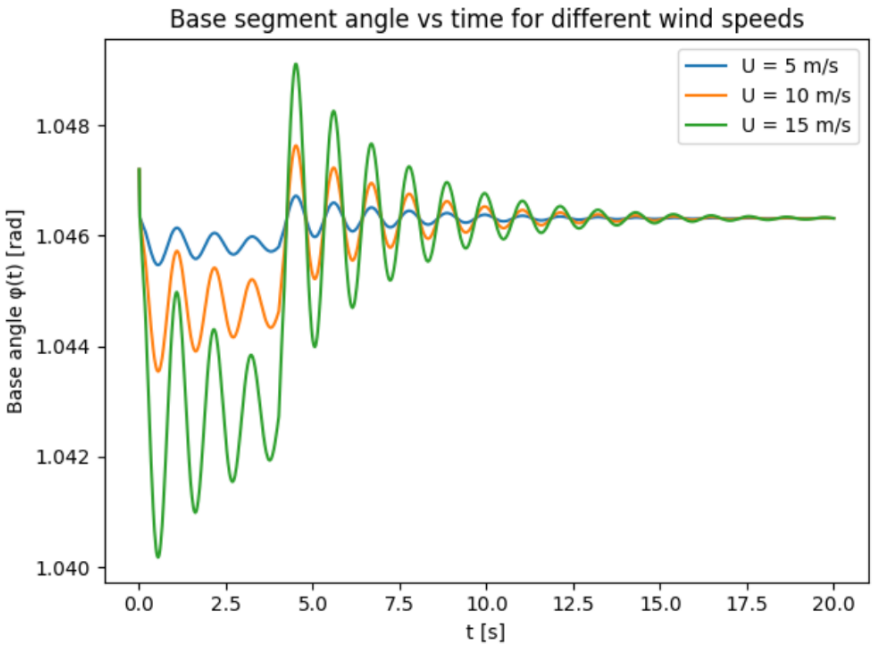

Figure 4: Base-segment angle $\phi(t)$ for three wind speeds.

4.4 Wind-load time history

Figure 5 illustrates the equivalent nodal wind force at the tip for the three wind speeds. Because the wind gust is modelled as a step-like distributed load applied for $0 \leq t \leq 4$ s and then removed, the resulting tip force histories are piecewise constant in time, with magnitudes proportional to U^2. The clear separation between the 5, 10 and 15 m/s cases emphasises that the differences in structural response arise solely from the aerodynamic loading, since all structural parameters are identical across the simulations.

While this simplified loading model neglects unsteady aerodynamic effects such as vortex shedding or fluctuating gust profiles, it is sufficiently rich to excite the dominant bending modes of the ladder and to reveal how the passive base damping copes with sudden changes in lateral load.

4.5 Maximum tip displacement versus wind speed

To condense the parametric influence of wind speed into a single measure, Figure 3 plots the maximum horizontal tip displacement (relative to the long–time equilibrium position) as a function of U. Over the investigated range the relationship is monotonic and close to quasi-linear: tripling the wind speed from 5 to 15 m/s increases the peak tip deviation by roughly a factor of six.

In practical terms, a 15 m/s lateral wind (equivalent to strong breeze / near–gale conditions) produces a tip swing of about 1.3 m in this model, which would be clearly perceptible to operators and potentially hazardous for precision tasks. The results therefore support the concern raised in the literature that extended ladders are highly sensitive to wind loading, and that even relatively modest gusts can induce large lateral motions if not adequately damped.

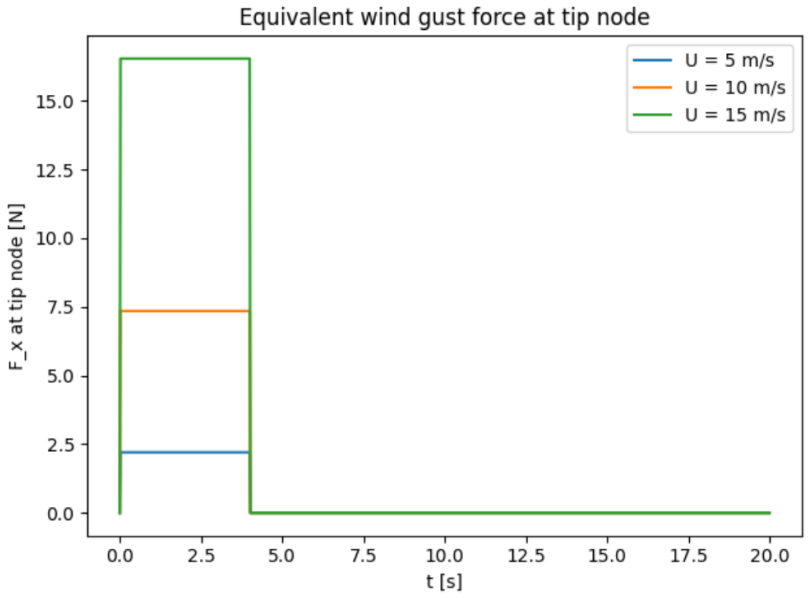

Figure 5: Equivalent horizontal wind force at the tip node.

4.6 Deformed ladder shapes under wind loading

Although the ladder remains approximately straight in the present simulations (because of the relatively high effective bending stiffness), snapshots of the deformed shapes at selected times provide useful qualitative insight into the response. For $U = 10$ m/s, shape plots at $t = 2$ and 4 s (within the gust duration) show a slight translation and rotation of the entire ladder in the wind direction, with only small curvature developing along the span. At later times ($t = 8$, 12 and 20 s) the amplitude of this lateral deflection progressively decays, and the configuration converges to a nearly straight line at a slightly shifted equilibrium position.

Comparing the shape snapshots for $U = 5$ and $U = 15$ m/s (not all shown here) reveals the same qualitative pattern but with different amplitude: the stronger wind case produces a visibly larger horizontal offset of the tip and a more pronounced oscillatory motion immediately after the load is removed. The fact that no significant local kinks or inflection points appear along the ladder confirms that, within the chosen parameter range, the first bending mode dominates the response and higher modes remain weakly excited.

4.7 Discussion and limitations

Overall, the numerical results indicate that the chosen passive base damping can substantially reduce wind-induced oscillations of a 20 m aerial ladder, bringing tip motions back to within a few centimetres in roughly 10–12 s after a gust event. The dependence of peak displacement on wind speed is strong: increasing U from 5 to 15 m/s changes the peak tip swing from a modest 0.2 m to more than 1 m, which is consistent with reported operational difficulties under strong cross-winds.

At the same time, several modelling simplifications must be acknowledged. The aerodynamic loading is represented by a quasi-steady, uniform drag model without spatial or temporal fluctuations; in reality, ladders experience turbulent gusts, partial shielding and possible vortex-induced vibrations. The equivalent homogeneous beam ignores local truss flexibility and joints, which may introduce additional modes and damping mechanisms. Finally, the torsional base joint is purely passive and linear in the present study; the literature suggests that semi-active or fully active modulation of the base damping could further reduce oscillation amplitudes, particularly for longer ladders and more

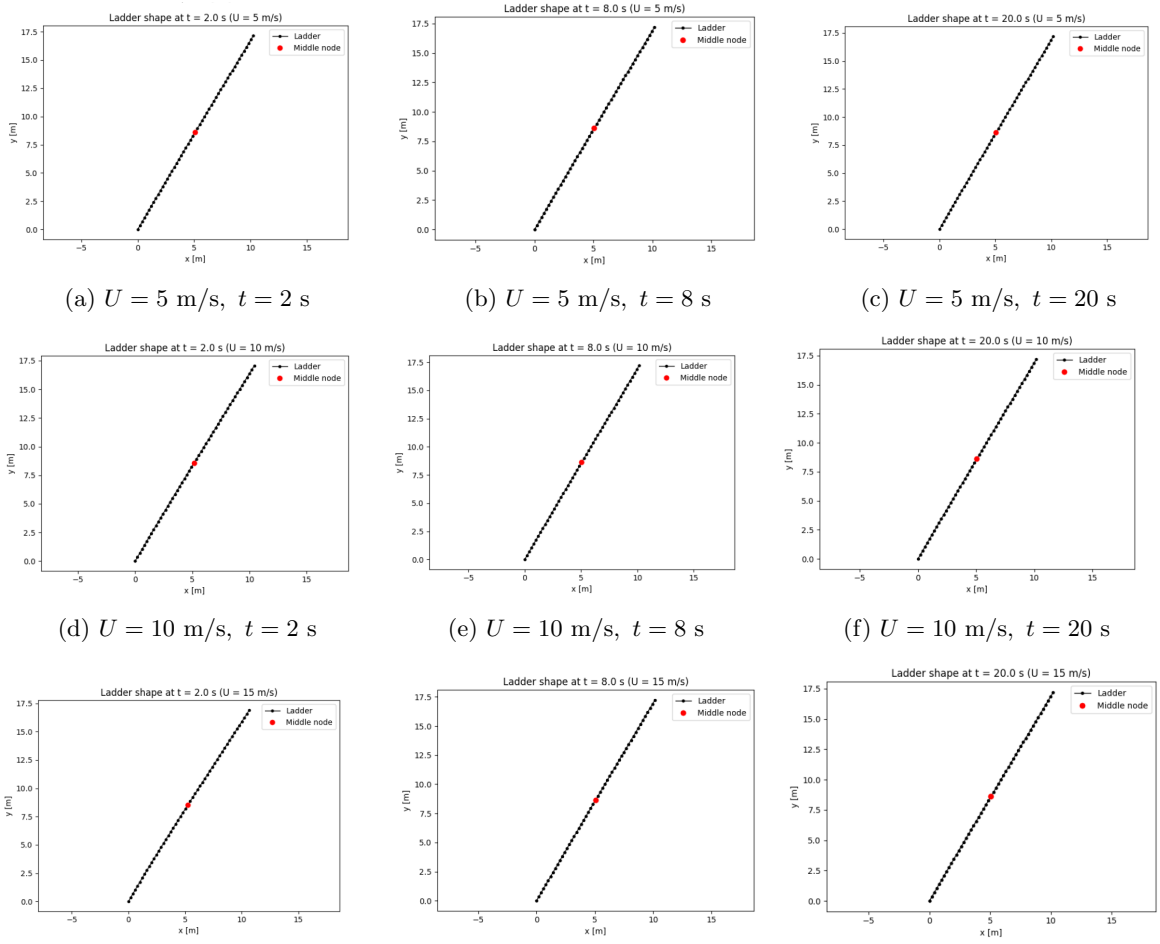

(a) $U = 5$ m/s, $t = 2$ s (b) $U = 5$ m/s, $t = 8$ s (c) $U = 5$ m/s, $t = 20$ s

(d) $U = 10$ m/s, $t = 2$ s (e) $U = 10$ m/s, $t = 8$ s (f) $U = 10$ m/s, $t = 20$ s

(g) $U = 15$ m/s, $t = 2$ s (h) $U = 15$ m/s, $t = 8$ s (i) $U = 15$ m/s, $t = 20$ s

Figure 6: Ladder shape snapshots for different wind speeds and times.

severe wind conditions.

Despite these limitations, the results provide a coherent framework for understanding the coupled influence of wind speed, Reynolds number and passive base damping on the dynamic behaviour of an aerial ladder. The current passive configuration forms a useful baseline against which future semi-active or active control strategies can be evaluated.

References

[1] P. Horvath, F. Hajdu, and R. Kuti, "Investigation of swings caused by sudden wind loads during operation of an aerial ladder.," *FME Transactions*, vol. 48, no. 2, 2020.

[2] S. H. H. Lavassani, R. Doroudi, and S. A. M. Gavgani, "Optimization of semi-active tuned mass damper inerter for enhanced vibration control of jacket platforms using multi-objective optimization due to environmental load," *Structures*, vol. 78, p. 109305, 2025.

[3] A. Kharitonov, N. Zimmert, and O. Sawodny, "Active oscillation damping of the fire-rescue turntable ladder," in *2007 IEEE International conference on control applications*, pp. 391–396, IEEE, 2007.

[4] H. Aschemann, O. Sawodny, A. Bulach, and E. P. Hofer, "Model-based trajectory control of a flexible turntable ladder," in *Proceedings of the American Control Conference*, pp. 921–926, 2002.

[5] A. Zuyev and O. Sawodny, "Stabilization of a flexible manipulator model with passive joints," in *Proceedings of the 16th IFAC World Congress*, (Prague, Czech Republic), 2005.

[6] S. A. Frank, *Control theory tutorial: basic concepts illustrated by software examples.* Springer Nature, 2018.